

### Design optimization of tumor vasculature-bound nanoparticle

I. Chamseddine, H.B. Frieboes,  
M. Kokkolaras

G-2018-36

May 2018

---

La collection *Les Cahiers du GERAD* est constituée des travaux de recherche menés par nos membres. La plupart de ces documents de travail a été soumis à des revues avec comité de révision. Lorsqu'un document est accepté et publié, le pdf original est retiré si c'est nécessaire et un lien vers l'article publié est ajouté.

**Citation suggérée:** I. Chamseddine, H.B. Frieboes, M. Kokkolaras (Mai 2018). Design optimization of tumor vasculature-bound nanoparticle, document de travail, Les Cahiers du GERAD G-2018-36, GERAD, HEC Montréal, Canada.

**Avant de citer ce rapport technique,** veuillez visiter notre site Web (<https://www.gerad.ca/fr/papers/G-2018-36>) afin de mettre à jour vos données de référence, s'il a été publié dans une revue scientifique.

The series *Les Cahiers du GERAD* consists of working papers carried out by our members. Most of these pre-prints have been submitted to peer-reviewed journals. When accepted and published, if necessary, the original pdf is removed and a link to the published article is added.

**Suggested citation:** I. Chamseddine, H.B. Frieboes, M. Kokkolaras (May 2018). Design optimization of tumor vasculature-bound nanoparticle, Working paper, Les Cahiers du GERAD G-2018-36, GERAD, HEC Montréal, Canada.

**Before citing this technical report,** please visit our website (<https://www.gerad.ca/en/papers/G-2018-36>) to update your reference data, if it has been published in a scientific journal.

---

La publication de ces rapports de recherche est rendue possible grâce au soutien de HEC Montréal, Polytechnique Montréal, Université McGill, Université du Québec à Montréal, ainsi que du Fonds de recherche du Québec – Nature et technologies.

Dépôt légal – Bibliothèque et Archives nationales du Québec, 2018  
– Bibliothèque et Archives Canada, 2018

The publication of these research reports is made possible thanks to the support of HEC Montréal, Polytechnique Montréal, McGill University, Université du Québec à Montréal, as well as the Fonds de recherche du Québec – Nature et technologies.

Legal deposit – Bibliothèque et Archives nationales du Québec, 2018  
– Library and Archives Canada, 2018

---

GERAD HEC Montréal  
3000, chemin de la Côte-Sainte-Catherine  
Montréal (Québec) Canada H3T 2A7

Tél. : 514 340-6053  
Télec. : 514 340-5665  
info@gerad.ca  
www.gerad.ca



# Design optimization of tumor vasculature-bound nanoparticle

Ibrahim M. Chamseddine<sup>a,e</sup>

Hermann B. Frieboes<sup>b,c,e</sup>

Michael Kokkolaras<sup>a,d,e</sup>

<sup>a</sup> Department of Mechanical Engineering, McGill University, Montreal, Quebec, Canada

<sup>b</sup> Department of Bioengineering, University of Louisville, Louisville, KY, USA

<sup>c</sup> James Graham Brown Cancer Center, University of Louisville, Louisville, KY, USA

<sup>d</sup> GERAD – Group for Research in Decision Analysis, Montreal, Quebec, Canada

<sup>e</sup> Joint senior authors

ibrahim.chamseddine@mail.mcgill.ca

hermann.frieboes@louisville.edu

michael.kokkolaras@mcgill.ca

May 2018

Les Cahiers du GERAD

G–2018–36

Copyright © 2018 GERAD, Chamseddine, Frieboes, Kokkolaras

Les textes publiés dans la série des rapports de recherche *Les Cahiers du GERAD* n'engagent que la responsabilité de leurs auteurs. Les auteurs conservent leur droit d'auteur et leurs droits moraux sur leurs publications et les utilisateurs s'engagent à reconnaître et respecter les exigences légales associées à ces droits. Ainsi, les utilisateurs:

- Peuvent télécharger et imprimer une copie de toute publication du portail public aux fins d'étude ou de recherche privée;
- Ne peuvent pas distribuer le matériel ou l'utiliser pour une activité à but lucratif ou pour un gain commercial;
- Peuvent distribuer gratuitement l'URL identifiant la publication.

Si vous pensez que ce document enfreint le droit d'auteur, contactez-nous en fournissant des détails. Nous supprimerons immédiatement l'accès au travail et enquêterons sur votre demande.

The authors are exclusively responsible for the content of their research papers published in the series *Les Cahiers du GERAD*. Copyright and moral rights for the publications are retained by the authors and the users must commit themselves to recognize and abide the legal requirements associated with these rights. Thus, users:

- May download and print one copy of any publication from the public portal for the purpose of private study or research;
- May not further distribute the material or use it for any profit-making activity or commercial gain;
- May freely distribute the URL identifying the publication.

If you believe that this document breaches copyright please contact us providing details, and we will remove access to the work immediately and investigate your claim.

**Abstract:** Nanotherapy represents a promising approach to target tumors with anticancer drugs while minimizing systemic toxicity. Evaluation of nanoparticle (NP) designs could benefit from computational analyses. Here, an optimization study was performed using an existing tumor model to find NP size and ligand density that maximize tumoral NP accumulation while minimizing tumor size. Optimal NP avidity lies at lower bound of feasible values, suggesting reduced ligand density to prolong NP circulation. For the given set of tumor parameters, optimal NP diameters were 288 nm to maximize NP accumulation and 334 nm to minimize tumor diameter, leading to uniform NP distribution and adequate drug load. Results further show higher dependence of NP biodistribution on the NP design rather than on tumor morphological parameters. A parametric study with respect to drug strength was performed. The weaker the drug, the bigger the difference is between the maximizer of NP accumulation and the minimizer of tumor size, indicating the existence of a specific drug strength that minimizes the differential between the two optimal solutions. This study shows the feasibility of applying optimization to NP designs to achieve efficacious cancer nanotherapy, and offers a first step towards a quantitative tool to support clinical decision making.

**Keywords:** Mathematical oncology, derivative-free optimization, cancer nanotherapy

---

**Acknowledgments:** HBF acknowledges the contribution of Grace Mahlbacher and Elizabeth Ehlman to create a “blackbox” version of the model in [1] for use by this study. HBF further acknowledges partial support by the National Institutes of Health/National Cancer Institute Grant R15CA203605. MK acknowledges partial support by Natural Sciences and Engineering Research Council Discovery Grant 436193-2013. These supports do not constitute an endorsement by the sponsors of the opinions expressed in this article.

## 1 Introduction

Targeted cancer nanotherapy relies on nanocarriers to deliver anticancer agents safely to tumors while minimizing systemic toxicity. Nanocarrier-mediated drug delivery has been associated with up to an 8-fold increase in drug efficacy compared to conventional chemotherapy [2]. Both drug and nanocarrier design play important roles in treatment efficacy. In general, drug design focuses on finding compounds that inhibit cancerous cell viability or proliferation, while nanocarrier design aims at developing nano-vehicle structures that maximize drug concentration in tumor relative to healthy tissue, thus reducing adverse drug effects. Experimental and computational methods have been employed to pursue such designs.

Specifically for vasculature-bound nanoparticles, *in vitro* studies have focused on characterizing the effect of nanocarrier design on margination, adhesion, and uptake while flowing through the tumoral vasculature. The tendency for vascular-borne liposomes and metal nanoparticles to drift from the blood streamlines towards the tumor vessel walls was studied by Toy et al. [3] using an *in vitro* microcirculation model. Considering different designs that vary in nanocarrier diameter {56, 60, 65, 100, 300 nm} as well as aspect ratio {0.45, 1}, it was shown that small eccentric nanoparticles are associated with stronger margination tendency. Larger nanoparticles, however, have exhibited a different correlation. Charoenphol et al. [4] examined the margination of nanoparticles of larger diameters {200, 500, 2000, 5000 nm}, flowing in an *in vitro* parallel flow chamber, showing that the margination rate increases with size. Patil et al. [5] measured *in vitro* the adherence strength of nanoparticles with diameters {5, 10, 15, 2  $\mu\text{m}$ } coated with P-selectin glycoprotein ligands, showing that large nanoparticles have strong adherence properties due to a high contact area with the vascular endothelium. Importantly, large nanoparticles are subjected to stronger hemodynamic forces and torques that may dissociate them from vessel walls [6]. Boso et al. [7] measured the accumulation of nanoparticles of {0.75, 1, 2, 4, 6  $\mu\text{m}$ } diameters in a parallel flow chamber. Data was fitted using an artificial neural network to correlate nanoparticle accumulation and size. As the size increases, the accumulation increases until it saturates or starts declining after a certain diameter that ranges between 4 and 6  $\mu\text{m}$  depending on the wall shear rate. The study indicates the presence of moderate nanoparticle size that maximizes the adherence properties.

In addition to the aforementioned *in vitro* studies, *in vivo* investigations have evaluated the overall efficacy of nanoparticles in living subjects. Rostami et al. [8] showed that encapsulating doxorubicin (DOX) in H6-equipped nanocarriers trebles the inhibition of mammary gland tumors in a mouse model compared to free DOX. Docetaxel-loaded nanoparticles of 349nm diameter were delivered to mouse mammary tumors in [9]. Significant improvement in antitumor activity was obtained by delivering the drug through nanoparticles. The effect of nanoparticle size was studied by Joshi et al. [10]. Liposomes of diameters {60, 80, 200, 650, 670 nm} delivered to gliomas have indicated that 200 nm had the highest uptake rate. Other *in vivo* studies are reviewed in Zhang et al. [11], for which nanoparticle design recommendations were based on increasing circulation time, taking advantage of the enhanced penetration and retention (EPR) effect, and maintaining high drug entrapment efficiency in the nanoparticle synthesis stage.

Quantifying nanotherapy efficacy using *in vitro* assays may require lengthy preparatory steps, which include setting up proper cell lines and reagents, synthesizing nanoparticles, and tailoring experimental protocols. The complexity of these studies is further escalated *in vivo*. The cost and time associated with *in vivo* studies present limitations to evaluating different designs. Not only is acquiring and maintaining animal models expensive, but there may exist a long process from the initiation of oncogenic mutation or transplantation of xenografts, tumor proliferation, to monitoring tumor regression after nanoparticle injection. This also requires advanced imaging techniques and multidisciplinary expertise. For these reasons, computational modeling offers an attractive option for exploratory evaluation of nanoparticle design that complements experimental work, including investigation of a wide range of variables.

Computational modeling of tumor growth and nanoparticle delivery is, however, non-trivial. Such models need to consider a variety of biological processes such as angiogenesis and drug cellular uptake in order to yield informative results. The models typically consist of submodels, coupled sequentially or iteratively, which may be difficult to solve and slow to converge to a solution. Decuzzi et al. [12] modeled the margination of nanoparticles by taking into consideration buoyant and hemodynamic forces, as well as van der Waals inter-

actions. The model explored a wide range of sizes, with results showing that diameters between 100 and 400 nm have relatively slower margination rates. Decuzzi and Ferrari [6] modeled the probability of nanoparticle adhesion at the vasculature wall. Parameters included nanoparticle size, aspect ratio, vessel wall shear stress, receptor-ligands association constant, ligand density, and receptor density. In parallel, tumor growth in two spatial dimensions coupled with neovasculature development was modeled mathematically in [13, 14, 15, 16]. In [17], Frieboes et al. integrated the nanoparticle delivery model of [6] with the tumor mechanics models of [15, 16] to create a comprehensive model to predict the intra-tumoral distribution and accumulation of vasculature-bound nanoparticles. However, the computational cost of the integrated model hinders the evaluation of all possible nanoparticle designs of interest. Nanospheres of {100, 600, 1000} nm diameters were simulated using different values of nanoparticle avidity and tumor conditions. The results showed that large nanoparticles accumulate at higher rates at the tumor periphery, while smaller nanoparticles have lower adherence strength but are distributed more uniformly throughout the tumor tissue. Van de Ven et al. [18] used the model in [16] to study the effect of drug strength on tumor growth inhibition and to determine the number of nanoparticles needed to reach a half maximal effective concentration  $IC_{50}$ . Wu et al. [19] used the model in [16] to study how the tumor interstitial pressure and fluid flow affect nanoparticle transport and distribution. Recently, the model in [17] was extended to simulate the tumor response to drug release from vasculature-bound nanoparticles [1]. Further information regarding mathematical characterizations of tumor nanotherapy can be found in [20, 21].

Previous computational and experimental work has primarily investigated the performance of nanocarriers using selected values of design variables such as nanoparticle size, aspect ratio, and ligand density. Optimizing nanoparticle design, however, requires design space exploration, which may be impractical to accomplish solely via empirical methods or computational models. Recently, Chamseddine and Kokkolaras [22] addressed this issue by applying rigorous optimization to the design of nanoparticles in order to maximize the tumoral nanoparticle accumulation and distribution with respect to the nanoparticle physical and chemical properties. The model was static, i.e., considered a single injection and does not update the tumor size and vasculature in response to the treatment. Although a sensitivity analysis was conducted to prove the robustness of the optimal design with 20% change in the average wall shear stress, the proposed design is not guaranteed to remain optimal if the tumor structure changes drastically. In this paper, optimization is applied to a “blackbox” version of the model, presented in [1], that considers the dynamic changes in the tumor size and vasculature, enabling to obtain a nanoparticle design that is potentially optimal over the course of treatment. This represents a first step toward the goal of developing a clinically-relevant numerical tool to assist nanoparticle design on a patient-specific basis.

## 2 Methods

### 2.1 Computational model

A previously developed numerical model is used to compute tumor growth and response to nanoparticle drug delivery. The model [1] builds upon the work of [6, 14, 15, 16, 17], and is used in this study as a “blackbox” system with a limited set of inputs to calculate nanoparticle accumulation and tumor regression as a function of the nanoparticle design. Briefly, the model is composed of 4 submodels that are coupled in the configuration shown in 1a [17]. The “Tumor Compartment” submodel computes the progression/regression of the tumor as a function of drug, oxygen, and nutrient concentrations. It also creates hypoxic and necrotic regions, which induce angiogenic factors (TAF). TAF drives the “Angiogenesis” submodel to develop new blood vessels. “Angiogenesis” is coupled with the “Flow” submodel, which determines the wall shear stress among other flow properties in the preexisting and neo-vasculatures. The “Nanoparticle” submodel determines the nanoparticle accumulation and drug release to the cancerous tissue as a function of the nanoparticle design and tumor parameters. Table 1 lists the input parameters to the “blackbox” system and their values as used in this study, unless it is otherwise specified in the text. The complete list of the computational model parameters is reported in [15, 16, 17, 1].

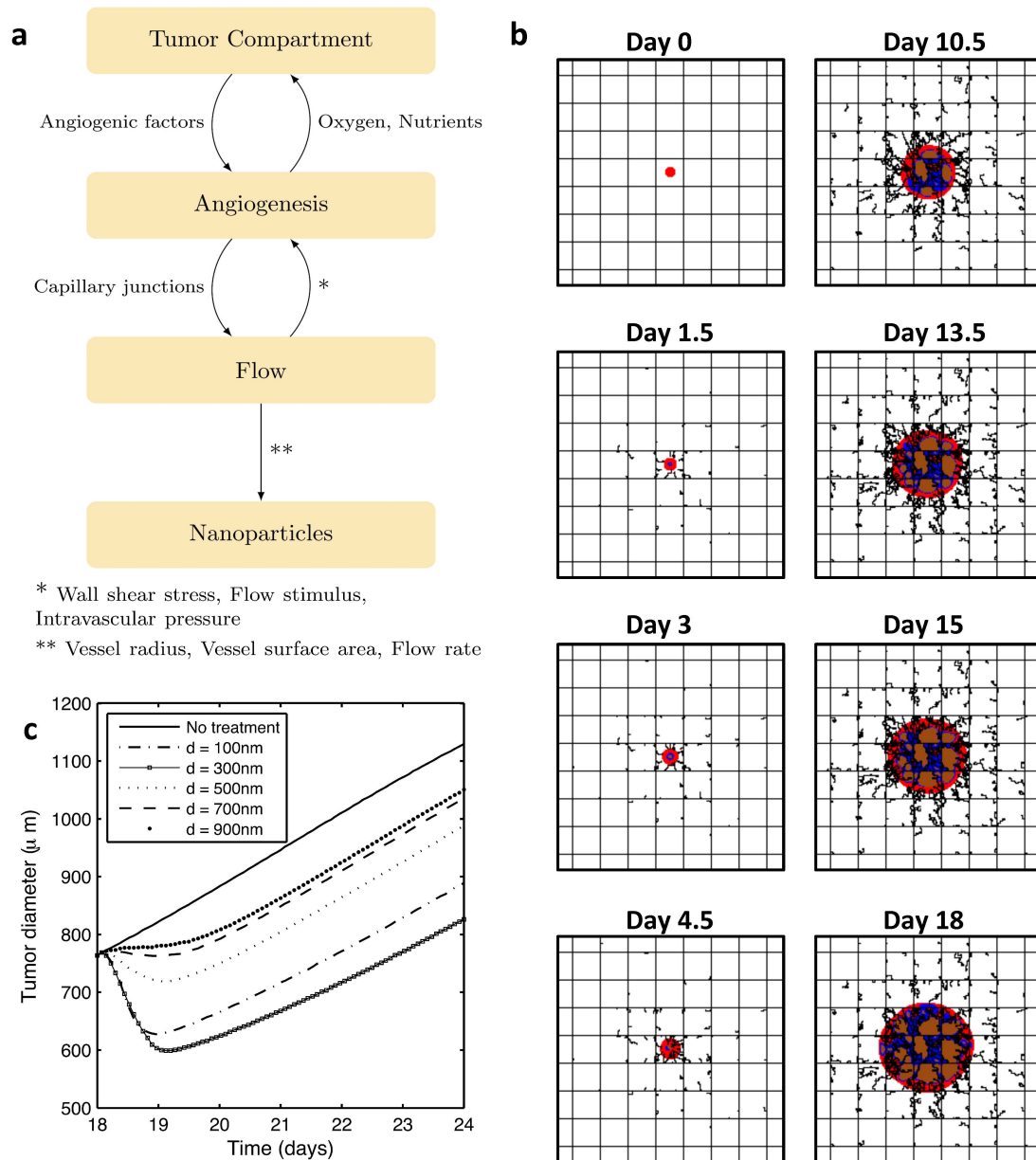


**Figure 1: Tumor model used for analysis. (a) Interaction among the different submodels as described in [17]. (b) Simulated tumor formation due to loss of growth control using the computational model. Viable, necrotic, and hypoxic tissues are represented in red, blue, and brown respectively. (c) Tumor regression in the treatment phase using different nanoparticle diameters.**

**Table 1: Main parameters used in the computational model.**

| Parameter  | Value                           |
|--|---------------------------------|
| Drug decay rate  | $4.1588s^{-1}$                  |
| Drug diffusion coefficient                                       | $3.334 \times 10^{-3}mm^2/s$    |
| Drug effect  | 1 (calibrated to moderate drug) |
| Measure of nanoparticle dissociation tendency ( $\beta$ in [17]) | $6.63 \times 10^{-4}m^{-2},s$   |
| Measure of receptor deficiency ( $\gamma$ in [17])               | $1.07 \times 10^3m^{-1.57}$     |
| Nanoparticle avidity ( $\alpha$ in [17])                         | $2.95 \times 10^{10}m^{-2}$     |

### 2.1.1 Growth phase

At day 0, a transformed group of cells is placed in the middle of a two-dimensional panel representing a tissue with blood vessels that are laid orthogonally as shown in Figure 1b to simulate the regular vascularization of normal tissue. Blood enters the tissue from the left and bottom sides to supply oxygen and nutrients. This enables the cancerous cells to proliferate and develop into a mass (tumor) due to the suppression of apoptosis. As the tumor grows, some cancerous cells distal from the blood vessels become hypoxic. This tissue produces TAF to stimulate new blood vessels that sprout from the existing vessels in order to supply the tumor tissue with blood. The neovasculature has an irregular structure and promotes tumor progression as shown in 1b. The growth phase is stopped at day 18 when the tumor reaches a diameter of  $780 \mu m$ , after which the treatment phase starts.

### 2.1.2 Treatment phase

Drug-carrying nanoparticles are injected into the blood vessel inlets at day 18. A fraction of the nanoparticles adhere to the tumor vessels. This fraction depends on the nanoparticle design. Anticancer agents are then released to the cancerous tissue. If the drug concentration exceeds a specific threshold, which depends on the drug strength (see Table 1), the tissue will die via apoptosis.

A preliminary investigation of a 6-day treatment phase was simulated using different nanoparticle diameters. The change in tumor diameter in response is depicted in Figure 1c. Since the curves do not intersect after 1 day of treatment, the treatment duration does not affect the relative performance for different nanoparticle sizes. Therefore, in our search for the optimal diameter, the treatment phase is stopped after 36 hours of nanoparticle injection, saving substantial computational time. Note that after a certain time of nanoparticle injection, a relapse is observed. This regrowth could be caused by two factors: either the drug is exhausted or the drug does not reach cytotoxic concentration for all of the proliferating tumor tissue.

## 2.2 Optimization

The ultimate goal of drug-based cancer treatments is to eradicate tumors completely or reduce their size prior to radical treatment intervention as a neoadjuvant therapy. Additionally, the aim of using nanoparticles as drug carriers is to reduce the side-effects associated with conventional chemotherapy while maximizing the drug delivery to the tumor tissue. Hence, we consider two objectives: minimizing the tumor size at the end of the treatment phase, and minimizing the treatment toxicity by maximizing the accumulation of nanoparticles in the tumor. Accordingly, two objective functions are defined:

1. Tumor Diameter (TD) : the tumor diameter at the end of the treatment (day 19.5) normalized to its value at the beginning of the treatment (day 18)
2. Tumor Nanoparticles (TNP) : the fraction of the injected nanoparticles that adhere to the tumor at the injection time (day 18)

Let  $\mathbf{x}$  denote the set of nanoparticle design variables. In general, the vector  $\mathbf{x}$  may include nanoparticle diameter, aspect ratio, elasticity, ligand density, ligand-receptor affinity constant, drug release rate, and drug load. In this study, we consider spherical nanoparticles (aspect ratio of 1) because they are easy to manufacture [23], and because they are predominant in current clinical and experimental studies [24, 25]. For instance, the clinically proven nanodrug Doxil - used to treat different types of cancers such as breast and ovarian - is composed of 100 nm spheres. The optimal values of  $\mathbf{x}$  that minimize TD, called minimizers of TD, can be obtained by solving:

$$\begin{aligned} \min_{\mathbf{x} \in \mathbb{R}^n} \quad & \text{TD}(\mathbf{x}) \\ \text{subject to} \quad & \mathbf{l}_b \leq \mathbf{x} \leq \mathbf{u}_b \\ \text{where} \quad & \mathbf{l}_b, \mathbf{u}_b \in \mathbb{R}^n, \end{aligned} \tag{1}$$

where  $n$  is the number of variables considered, and  $\mathbf{l}_b$  and  $\mathbf{u}_b$  are the lower and upper bounds that define the feasible region of  $\mathbf{x}$ . Constraints are implemented implicitly in the analysis model. The maximizers of TNP

are determined by solving:

$$\begin{aligned} & \max_{\mathbf{x} \in \mathbb{R}^n} && \text{TNP}(\mathbf{x}) \\ & \text{subject to} && \mathbf{l}_b \leq \mathbf{x} \leq \mathbf{u}_b \\ & \text{where} && \mathbf{l}_b, \mathbf{u}_b \in \mathbb{R}^n. \end{aligned} \tag{2}$$

Problems (1) and (2) are solved using the Mesh Adaptive Direct Search algorithm (MADS) [26]. Since the gradients of the computational model cannot be approximated reliably, we use MADS, which is a derivative-free optimization algorithm that has rigorous convergence properties. Moreover, the computational model used here as a blackbox for analysis is computationally expensive. To examine a single nanoparticle design, an Intel(R) Core(TM) i7-3770 CPU @ 3.4GHz processor requires 1.5 hours of CPU time. For this reason, we use a surrogate-assisted optimization approach to reduce the number of computational model evaluations required to obtain the optimal design. Specifically, we utilize the search step of the iterative mesh adaptive direct search (MADS) algorithm [27] to solve a surrogate of the optimization problem, i.e., we solve the optimization problem using surrogate models of the objective functions. To enhance the efficiency of the MADS algorithm we build and update ensembles of surrogates and use a novel order-based error metric tailored specifically for surrogate optimization to utilize the best surrogate at each iteration [28]. In this manner, we generate several candidates for the next iterate, which we combine with the candidates generated at the poll step of MADS, which is the foundation of its convergence properties. The computational model is then used only to evaluate all these candidates opportunistically to select the next iterate. In other words, we generate a lot of useful information by means of computationally inexpensive surrogate models but make algorithmic decisions using the high-fidelity computational model.

### 2.3 Data availability

All data analysed during this study are included in this published article. Additional datasets generated are available from the corresponding author upon request.

## 3 Results

### 3.1 Optimizing nanoparticle diameter

The drug biodistribution depends on the diameter  $d$  of the drug-carrying nanoparticles, which are localized depending on their size [22, 17, 29]. Small nanoparticles are associated with longer circulation time, increasing their chance to reach the tumor. Their adherence properties are poor, however, due to the low contact area between ligands on the surface of the nanoparticles and receptors over-expressed in the vascular endothelium of the malignant lesion. On the other hand, large nanoparticles have strong binding affinity, but they are also exposed to high hemodynamic loadings that may dissociate them from the endothelium. In addition, large nanoparticles tend to accumulate at the periphery of the tumor or bind to healthy tissues before they reach the tumor site due to their low circulation time. The optimal nanoparticle diameter  $d^*$  lies within this range and is obtained by solving Problems (1) and (2) while setting  $\mathbf{x} = [d]$ . Nanoparticles smaller than 10 nm are exposed to renal clearance, and nanoparticles larger than 1000nm may not be able to flow in narrow tumor vessels and cause embolism. Therefore,  $d$  lies between  $\mathbf{l}_b = 10\text{nm}$  and  $\mathbf{u}_b = 1000\text{nm}$  in this study. For this evaluation, the nanoparticle avidity  $\alpha = 2.95 \times 10^{10} m^{-2}$ , calculated by considering typical values for the receptor density, ligand density, and receptor-ligand binding constant under zero load, which are in the order of  $10^{12} \# / m^2$ ,  $10^{14} \# / m^2$ , and  $10^{-14} m^2$  respectively [17].

Figure 2a compares empirically-selected points with MADS-selected points in an attempt to minimize TD. In empirical methods, trial points are randomly chosen; however, using MADS, trial points are selected systematically to converge to the optimal solution. Note that when MADS approaches the optimal diameter, it tries many points in the vicinity before terminating at the best solution. The obtained optimal nanoparticle diameter up to 1 nm accuracy is  $d^* = 190\text{nm}$ , reducing  $\text{TD}^* = 0.683$ .

Similarly, Problem (2) is solved to maximize the tumor nanoparticle accumulation. The progress of MADS is shown in Figure 2b. The optimal nanoparticle size that maximizes TNP is  $d^* = 147\text{nm}$  leading

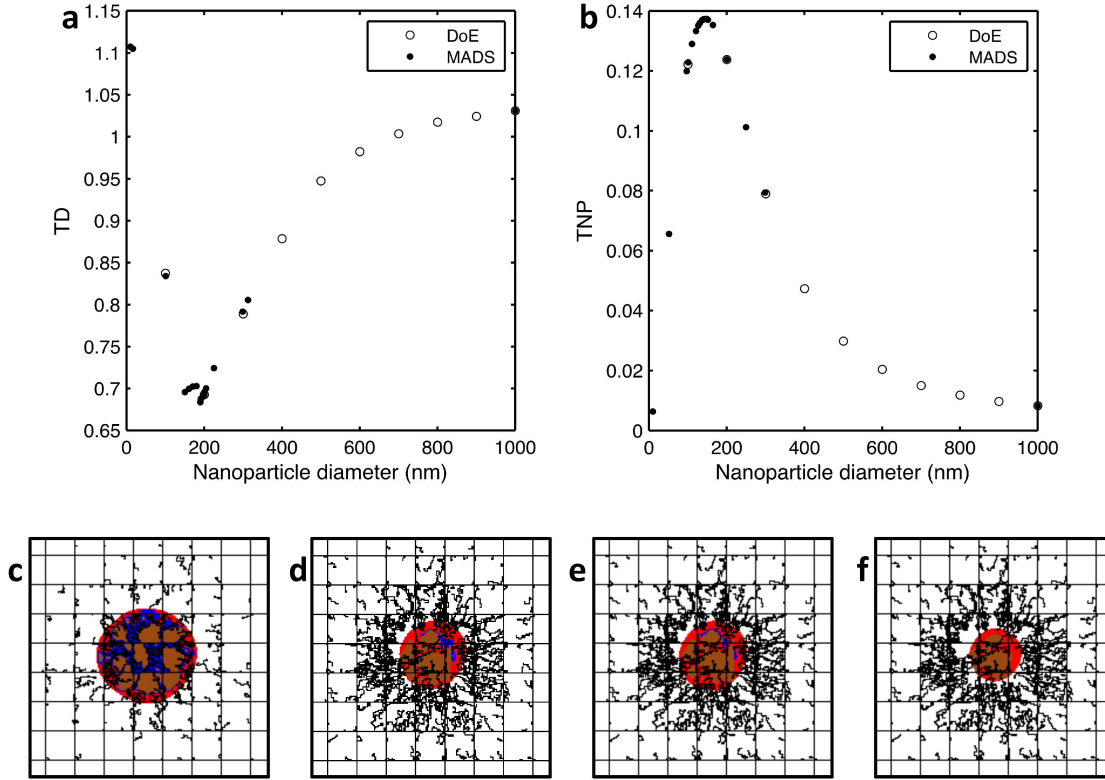


**Figure 2: Simulation of tumor treatment using optimal nanoparticle designs.** Comparison of MADS-selected points with sample designs selected manually to find the (a) minimizer of TD, and (b) maximizer of TNP. Simulated tumor (c) before treatment, (d) after 36 hours of treatment using the minimizer of TD  $d^* = 190\text{nm}$  showing a reduction to 68.3% of its initial diameter, (e) after 36 hours of treatment using the maximizers of TNP  $d^* = 147\text{nm}$  showing a reduction to 69.6% of its initial diameter, and (f) after 36 hours of treatment with nanoparticles of  $(d^* = 334\text{nm}, \alpha^* = 1e10m^{-2})$  obtained after expanding  $\mathbf{x}$  to  $[d, \alpha]$  showing a reduction to 50.5% of its initial diameter.

to  $\text{TNP}^* = 0.137$ ; i.e., around 14% of the injected nanoparticles successfully reach and adhere to the tumor. The corresponding TD is 0.484. Both optimal solutions are summarized in Table 2. Figure 2d,e shows the regression of the tumor by injecting both optimal solutions.

**Table 2: Solutions of Problems (1) and (2) with  $\mathbf{x} = [d]$ .**

|                 | Objective Function          | Optimizer            | Optimum                |
|-----------------|-----------------------------|----------------------|------------------------|
| <i>Minimize</i> | Tumor Diameter (normalized) | $d^* = 190\text{nm}$ | $\text{TD}^* = 0.683$  |
| <i>Maximize</i> | Tumor Nanoparticle Fraction | $d^* = 147\text{nm}$ | $\text{TNP}^* = 0.137$ |

### 3.2 Effect of nanoparticle avidity

Vasculature-bound nanoparticles are equipped with ligands of high binding affinity to receptors over expressed in the vascular endothelium of tumor vessels. In the model, we assume that the integrin  $\alpha_v\beta_3$  exists with an area density  $m_r$  in the malignant lesion. Corresponding ligands such as vitronectin [30], fibronectin [31], fibrinogen [32], and osteopontin [33] are available at the surface of the nanoparticles with density  $m_\ell$ . Each receptor-ligand pair has a certain affinity that is quantified by the binding constant under zero load  $K_A^0$ . The nanoparticle avidity  $\alpha \propto m_r m_\ell K_A^0$  corresponds to the overall affinity of the nanoparticle [17].

The optimization problems (1) and (2) are solved again using a different value of  $\alpha$  to check if the optimal diameters change. Changing the parameter  $\alpha$  has an effect on the optimal nanoparticle diameters as shown in Table 3, where the cases of  $\alpha = 1 \times 10^{11}m^{-2}$  and  $\alpha = 1 \times 10^{12}m^{-2}$  are listed. It can be observed that as  $\alpha$  increases, the diameter that maximizes TNP decreases. This decrease in  $d^*$  can be explained by the increased

ligand and receptor densities to the point that the nanoparticle-endothelium contact area required to cause binding is reduced. The minimal TD is altered, however, since smaller nanoparticles have lower drug loads. Since the value  $\alpha$  has an effect on the optimal nanoparticle diameter, it is necessary to add it to the set of variables to optimize it along with  $d$  in an all-in-one optimization problem.

**Table 3: Solutions of Problems (1) and (2) with  $\mathbf{x} = [d]$  using different values of  $\alpha$ .**

| Solution of                           | Problem (1)          |                       | Problem (2)          |                        |
|---------------------------------------|----------------------|-----------------------|----------------------|------------------------|
| $\alpha = 2.95 \times 10^{10} m^{-2}$ | $d^* = 190\text{nm}$ | $\text{TD}^* = 0.683$ | $d^* = 147\text{nm}$ | $\text{TNP}^* = 0.137$ |
| $\alpha = 1 \times 10^{11} m^{-2}$    | $d^* = 90\text{nm}$  | $\text{TD}^* = 0.866$ | $d^* = 69\text{nm}$  | $\text{TNP}^* = 0.137$ |
| $\alpha = 1 \times 10^{12} m^{-2}$    | $d^* = 230\text{nm}$ | $\text{TD}^* = 1.08$  | $d^* = 15\text{nm}$  | $\text{TNP}^* = 0.137$ |

### 3.2.1 Treating nanoparticle avidity as a design variable

Let  $\mathbf{x} = [d, \alpha]^T$ . The range of  $\alpha$  is assumed to be between  $10^{10}$  and  $10^{12} m^{-2}$  complying with typical ranges of  $m_r$ ,  $m_\ell$ , and  $K_A^0$  [6, 17]. Hence, the feasible design space is  $\mathbf{l}_b = [10\text{nm}, 10^{10} m^{-2}]^T$  and  $\mathbf{u}_b = [1000\text{nm}, 10^{12} m^{-2}]^T$ . Results for minimizing the tumor diameter and maximizing the tumor nanoparticle accumulation are shown in Table 4.

**Table 4: Solutions of Problems (1) and (2) with  $\mathbf{x} = [d, \alpha]^T$ .**

|                 | Objective Function          | Optimizer   | Optimum                |
|-----------------|-----------------------------|---|------------------------|
| <i>Minimize</i> | Tumor Diameter (normalized) | $[d^* = 334\text{nm}, \alpha^* = 10^{10} m^{-2}]$ | $\text{TD}^* = 0.505$  |
| <i>Maximize</i> | Tumor Nanoparticle Fraction | $[d^* = 288\text{nm}, \alpha^* = 10^{10} m^{-2}]$ | $\text{TNP}^* = 0.137$ |

Optimizing both nanoparticle diameter and avidity provides a better tumor reduction. Figure 2f displays the tumor at the beginning and end of the treatment, showing that the tumor reduces to 50.5% of its diameter at the start of treatment. Note that the optimal value of  $\alpha$  lies at its lower bound ( $10^{10} m^{-2}$ ) for both problems. The corresponding optimal diameter is increased to maintain an adequate contact area with the endothelium.

### 3.2.2 Relaxing the $\alpha$ -boundary constraint

The lower bound of  $\alpha$  is an active bound; i.e., if it changes, the optimal value of  $\alpha$  changes. To examine the proposed nanoparticle design practice of reducing the value of  $\alpha$  and selecting a proper diameter, we reduce the lower bound of  $\alpha$  to  $10^9 m^{-2}$  and check if  $\alpha^*$  remains a boundary optimum. Figure 3 plots MADS progression toward the optimal solution of the relaxed problem. The solution confirms the existence of  $\alpha^*$  at the active bound. The variable  $d^*$  remains an interior optimum having a value of 980 nm, increased to compensate for low ligand density.

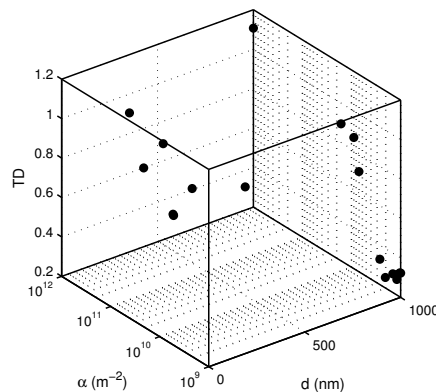


**Figure 3: The blackbox evaluation points showing that the design space has been sampled adequately with convergence to the optimal values of  $d$  and  $\alpha$  that minimize TD.**

### 3.3 Robustness of the optimal design

The solution for Problems (1) and (2) may change if the tumor morphology changes. Although numerical optimization can form a powerful tool that supports precision medicine dealing with patient-specific situations, designs that are aimed at treating a wide range of patients need to be insensitive to changes in tumor parameters. A rigorous method to attain robust designs is to optimize under uncertainty [34], which will be addressed in future work. Alternatively, we perform a sensitivity analysis with respect to model parameters that characterize the tumor microenvironment. We identify  $\beta$  and  $\gamma$  as candidates for altering the optimal design. The parameter  $\beta \propto \chi\mu/(k_B T m_r)$  combines Boltzmann thermal energy, blood viscosity, ligand-receptor binding force, and receptor density. The parameter  $\gamma$  is inversely proportional to the receptor density. More details about these parameters can be found in [6, 17].

Let  $Z_d, Z_\alpha, Z_\beta, Z_\gamma$  be categorical variables that measure  $d, \alpha, \beta,$  and  $\gamma$  respectively. Each categorical variable has a value that belongs to the set  $\{1, 2, 3\}$  referring to  $\{\text{Low, Medium, High}\}$ . For example, the set  $Z_d = \{1, 2, 3\}$  refers to  $\mathbf{d} = \{10, 500, 1000\}nm$ . Similarly,  $Z_\alpha = \{1, 2, 3\}$  means  $\alpha = \{1e10, 1e11, 1e12\}m^{-2}$ . Considering 3 levels for four variables, there exist 81 permutations of the vector  $[Z_d, Z_\alpha, Z_\beta, Z_\gamma]^T$ .

The parameters  $\beta$  and  $\gamma$  are expected to have a direct impact on nanoparticle accumulation because they model nanoparticle-to-endothelium interactions. Therefore, we investigate the change in TNP with respect to the input vector using the interaction plot of Figure 4. The interaction plot is a matrix plot, where the diagonal of the plot displays the categorical variables. The interaction of the parameter highlighted at the row-diagonal (i,i) with the parameter at the column-diagonal (j,j) is displayed at the off-diagonal position (i,j). For instance, the subplot (1,2) plots the interaction of  $d$  and  $\alpha$ . The horizontal axis is  $Z_\alpha$ , the vertical axis is the output TNP, and the different lines are the different values of  $Z_d$  (indicated on the legend to the right of the corresponding row). The contribution of  $\beta$  and  $\gamma$  is illustrated in the subplots (1,3), (1,4), (2,3), (2,4), (3,1), (3,2), (3,4), (4,1), (4,2), and (4,3). In all of these plots, the graphs are either horizontal or coincide. Therefore, nanoparticle accumulation highly depends on the nanoparticle design and less on tumor biological conditions such as receptor density and blood properties.

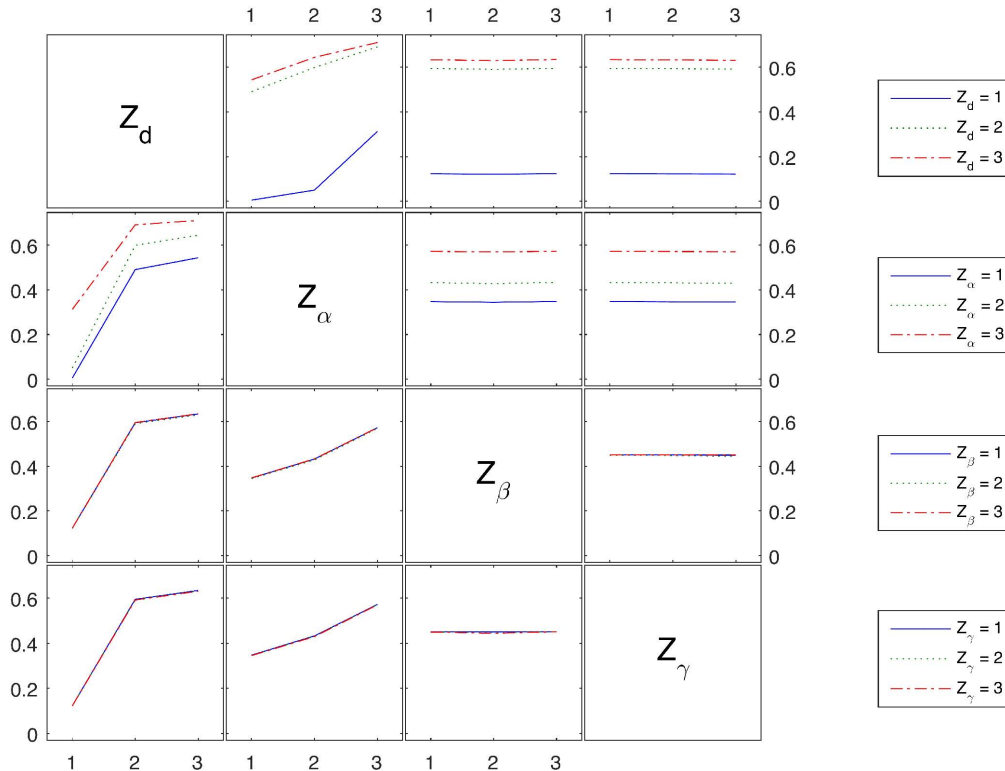


Figure 4: Interaction plot of  $d, \alpha, \beta,$  and  $\gamma$  with the output TNP.

### 3.4 Effect of drug efficacy

The efficacy of the drug encapsulated in the nanoparticles has an important role in tumor regression [18]. Strong drugs cause fast shrinkage but are associated with high systemic toxicity. On the other hand, weak drugs may evince slower tumor regression but have higher median toxic dose, lowering the associated adverse events. The computational model accounts for the drug efficacy through the proliferative term  $\lambda_p = [\sigma(1 - \bar{\lambda}_{effect}\bar{C}_D\mathbf{1}_{D>T_{drug}}) - A]$ , which quantifies the interplay between cell mitosis, promoted by the availability of nutrients and oxygen  $\sigma$ , and cell apoptosis, which occurs if the drug concentration  $D$  exceeds a specific threshold  $T_{drug}$  in the tissue [18, 1]. The drug strength is measured by  $\bar{\lambda}_{effect}$  having a unit of effect per drug concentration. The parameter  $C_D$  is a rescaling factor and  $A$  is the natural apoptosis rate.

In Section 3.2.1, a hypothetical drug of moderate efficacy was used. The parameter  $\bar{\lambda}_{effect}$  was normalized to 1 for the drug considered. Stronger drugs are characterized by  $\bar{\lambda}_{effect} > 1$ , while weaker drugs have a value of  $\bar{\lambda}_{effect}$  between 0 and 1. Although drug efficacy does not affect nanoparticle accumulation, it has an impact on the amount of drug needed to induce cell apoptosis, which is expected to change the minimizers of TD.

It was shown in Section 3.1 that there is a difference between the optimal diameter  $d_{TD}^*$  that minimizes TD and  $d_{TNP}^*$  that maximizes TNP. Figure 5a plots both optimal diameters for the case of  $\alpha = 1 \times 10^{10}m^{-2}$ . If nanoparticles are smaller than  $d_{TD}^* = 334nm$ , less drug is released to the tissue and thus TD is higher. If nanoparticles are larger than  $d_{TD}^* = 334nm$ , they aggregate toward the tumor margin, reducing the tumor diameter exposed to the drug. If nanoparticles are smaller than  $d_{TNP}^* = 288nm$ , their probability to adhere to the tumor site is lower due to the small contact area between the nanoparticle and tumor vessel wall. If nanoparticles are larger than  $d_{TNP}^* = 288nm$ , they are exposed to higher dissociative hemodynamic loadings that return them to the bloodstream. Between the two optimal solutions  $d_{TNP}^* = 288nm$  and  $d_{TD}^* = 334nm$ , there exists a region where the treatment shows the most favorable outcome. In this desired region, the nanoparticle design can be selected depending on the weight given to each treatment attribute - lower toxicity versus faster treatment.

#### 3.4.1 Parametric study with respect to drug efficacy

Figure 5 implies that the maximal therapeutic potential is not necessarily tied to the maximal nanoparticle accumulation. In fact, depending on drug efficacy, a smaller number of large nanoparticles can cause better tumor reduction than smaller nanoparticles. This defines the shaded zone of Figure 5a. The case of a weaker drug ( $\bar{\lambda}_{effect} = 0.5$ ) is then considered to investigate the change in the  $d_{TD}^*$ . The shaded zone becomes wider since  $d_{TD}^*$  is increased to 384nm to provide higher drug volume needed in the tissue (Figure 5b).

In addition, a stronger drug is studied by setting  $\bar{\lambda}_{effect}$  to 2. Figure 5c shows that the width of the shaded region decreases. If  $\bar{\lambda}_{effect}$  increases further to 5, the minimizer of TD becomes less than the maximizer of TNP. The reason is that a large drug load per nanoparticle is not needed to cause apoptosis at high values of  $\bar{\lambda}_{effect}$ . Therefore, the optimal solution shifts to small nanoparticles because they distribute more uniformly.

Notably, in all the considered cases, a small sacrifice in TNP leads to an increase in TD. Therefore, from a computational point of view, nanoparticle designs should be driven by minimizing TD. However, this conclusion may not be generalized; it requires extensive experimental support and should be evaluated for specific tumors. Furthermore, the reason TNP is less sensitive to the nanoparticle design could be due to an implicitly specified model parameter. Finding the drug efficacy that produces unified optimizers for both objective functions provides an indication of the drug strength that removes a foreseen tradeoff between treatment speed and toxicity.

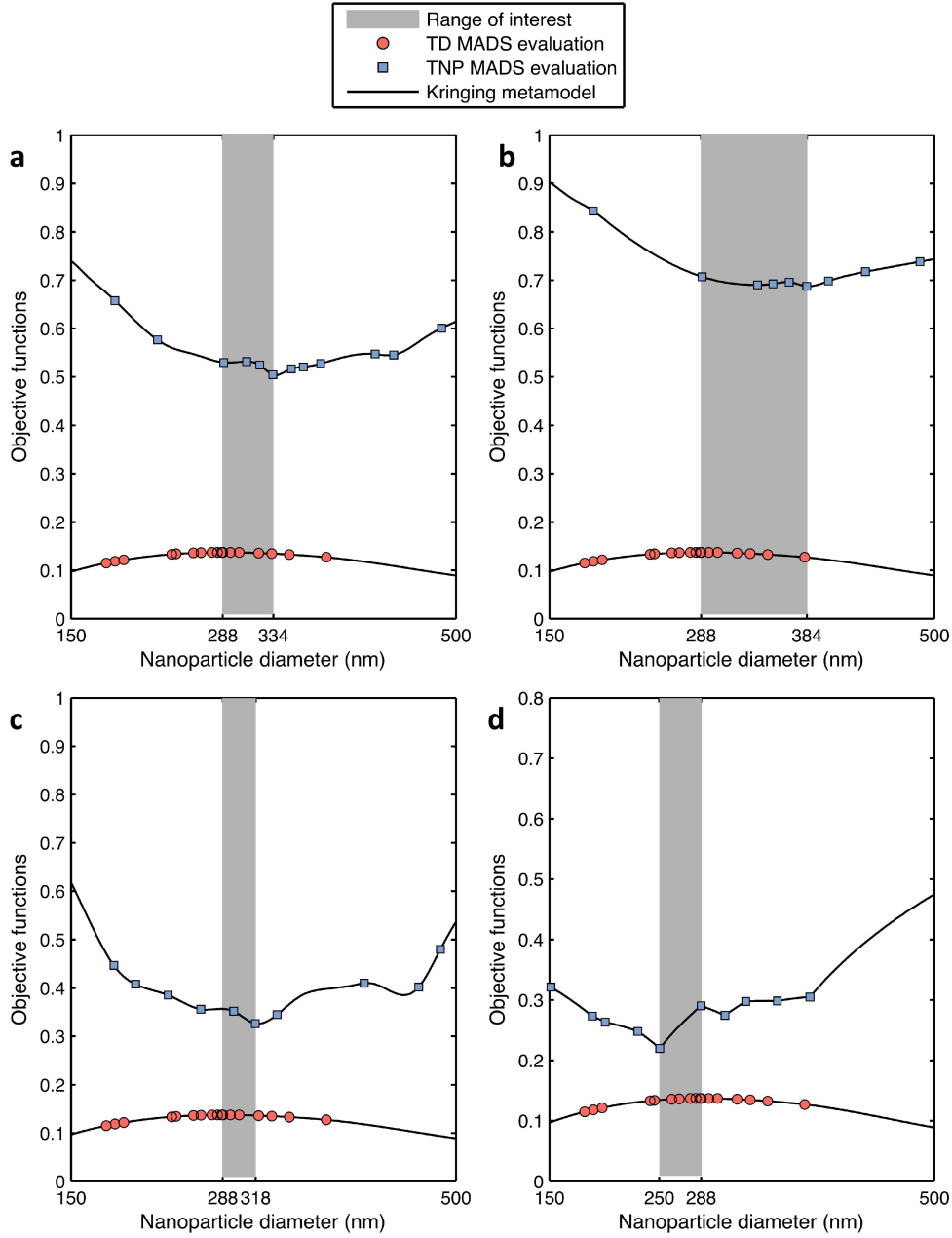


**Figure 5: Effect of drug efficacy on the optimal nanoparticle design. Optimal nanoparticle diameters and local variations at  $\alpha = 1e10m^{-2}$  and (a)  $\bar{\lambda}_{effect} = 1$ , (b)  $\bar{\lambda}_{effect} = 0.5$ , (c)  $\bar{\lambda}_{effect} = 2$ , and (d)  $\bar{\lambda}_{effect} = 5$ .**

### 3.4.2 Conjugating $d_{TD}^*$ and $d_{TNP}^*$

In order to find a single nanoparticle diameter that optimizes both objective functions, we define the optimization problem

$$\begin{aligned}
 & \min_{\bar{\lambda}_{effect} \in \mathbb{R}} && (d(\bar{\lambda}_{effect}) - \text{argmax}(\text{TNP}))^2 \\
 & \text{subject to} && 0.2 \leq \bar{\lambda}_{effect} \leq 10 \\
 & \text{where} && d = \text{argmin}(\text{TD} |_{\bar{\lambda}_{effect}}) \\
 & && \text{argmax}(\text{TNP}) = 288\text{nm}.
 \end{aligned} \tag{3}$$

Problem 3 tries to find the drug efficacy at which the minimizer of TD coincides with the maximizer of TNP (288 nm). Solving Problem (3) requires two loops. The inner loop computes  $d_{TD}^*$  given a drug efficacy  $\bar{\lambda}_{effect}$  that is specified by the outer loop. The outer loop iterates to minimize the difference between  $d_{TD}^*$  and 288 nm with respect to  $\bar{\lambda}_{effect}$ . In each outer loop iteration, the inner loop has to complete a full optimization process to find the minimizer of TD. The nested nature of Problem (3) requires extensive computational time, which could exceed a month if the computational model used as a blackbox for analysis is used. Alternatively, a surrogate model is created by fitting the points that were evaluated earlier. Figure 6a shows the kriging metamodel constructed using the DACE (Design and Analysis of Computer Experiments) [35]. Exponential correlation functions and second-order polynomial regression models are employed to generate the kriging metamodel.

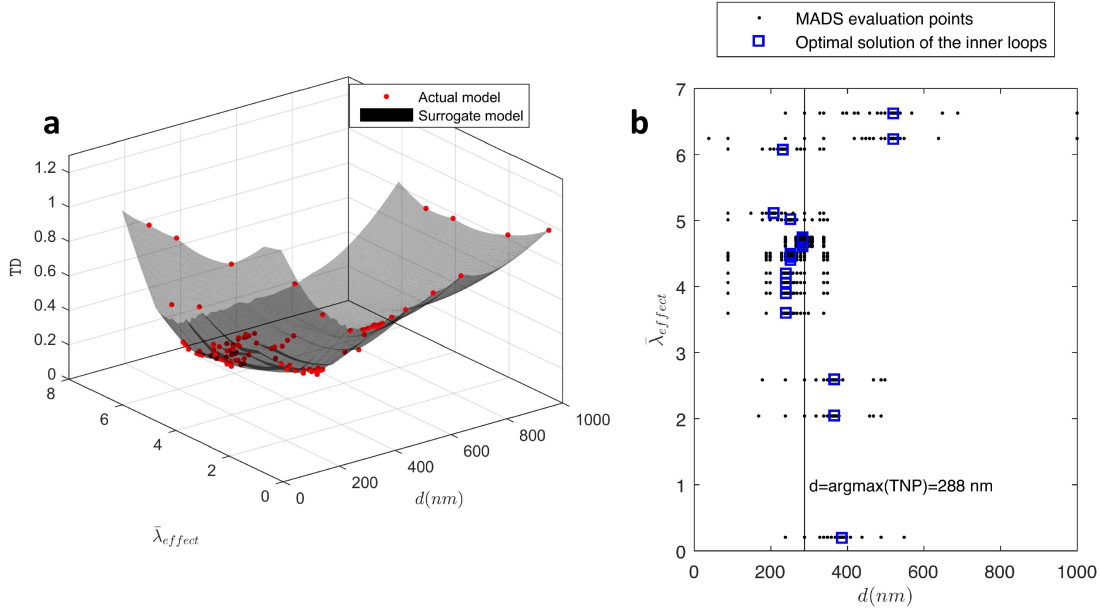


**Figure 6: Optimization of drug efficacy. (a) Surrogate of the true model synthesized using kriging method of interpolation. (b) Progress of MADS in solving the inner and outer loops of problem (3).**

The solution process of Problem (3) is illustrated in Figure 6b. Each inner loop has a fixed value of  $\bar{\lambda}_{effect}$  on the vertical axis. Given  $\bar{\lambda}_{effect}$ , MADS visits the surrogate model and finds  $d$  that is closest to 288 nm, marked by the vertical line in the plot. The inner loop iterates horizontally to converge to the optimal solutions, shown in crosses. Then  $\bar{\lambda}_{effect}$  changes in the outer loop and the same procedure repeats until the optimal solution  $\bar{\lambda}_{effect}^*$  is obtained. The minimal difference between  $d_{TD}^*$  and  $d_{TNP}^*$  is 6 nm. It is attained at the optimal drug efficacy  $\bar{\lambda}_{effect}^* = 4.7$ , where the minimizer of tumor diameter is 282 nm, which corresponds to 27% of the tumor diameter at the start of treatment.

## 4 Discussion

This study applies optimization to the design of drug-carrying nanoparticles targeting tumor vascular-endothelium. Empirical methods to obtain optimal designs are typically based on trial and error schemes. Instead, an optimization approach systematically converges to the optimal design using a significantly lower number of trial points. The reduction in computational time is necessary since optimal solutions are subject to change due to variations in tumor morphology, patient status, and cancer type [36]. Our previous study [22] was a first attempt to engage rigorous numerical optimization with the design of nanoparticles. We based our analysis on a model that simulates the distribution of nanoparticles and drug release to the tissue without considering the tumor response. In this study, we combined the optimization technique of [22] with a computational model of tumor nanotherapy [1] that models tumor evolution and includes complex biological processes such as angiogenesis and tissue necrosis [14, 15, 16, 17]. This enables more reliable nanoparticle designs that are optimal for the whole duration of the treatment.

First, the nanoparticle diameter was optimized. Previous studies have predicted that the optimal design moderately lies between lower, more uniform nanoparticle distribution, and higher less uniform distribution [17, 1, 37]. Experimental studies have examined a finite set of diameters to approximate the ideal size using *in vitro* and *in vivo* studies as reviewed in Section 1 and in [38, 39]. Computationally, various diameters were investigated to correlate nanoparticle size and pharmacokinetics [29]. In [17], three diameters were studied ( $\{100, 600, 1000\}$  nm). The respective tumor accumulation was  $\{12.2\%, 2\%, 0.8\%\}$ . In comparison, the optimal diameter of 147 nm obtained in this study yielded accumulation of 13.7%.

The set of design variables has been expanded to include nanoparticle avidity because it has an impact on nanoparticle distribution [40]. Multidimensional search schemes give rigorous optimization a computational advantage over brute force methods that change one variable at a time. Optimizing nanoparticle diameter and avidity in an all-in-one problem shows a 1.6-fold decrease in tumor diameter and the same percent of nanoparticle accumulation as compared to optimizing the nanoparticle diameter alone. The resulting optimal diameters that maximize tumor targeting and minimize tumor diameter are 288 nm and 344 nm respectively. These diameters lie in the range that benefit from the EPR effect [7].

The values of the optimal solution have a significant physical meaning. Previous studies have discussed that one way to prolong nanoparticle circulation is size reduction [41, 42, 43]. The results suggest that decreasing the nanoparticle avidity is a substitute approach in order to leverage the therapeutic potential of larger nanoparticles (of higher drug load). To further investigate, we reduced the lower bound of the nanoparticle avidity. The results confirm the existence of optimal nanoparticle avidity at the lower bound, whereas the optimal nanoparticle diameter increased to compensate for the decrease in the ligand-receptor pairing per unit area. This conclusion is specific for vasculature-bound nanoparticles where the drug is released at the endothelial layer. For the case where nanoparticles internalize to the tissue, smaller nanoparticles show higher cellular uptake rate, as reported in [44, 45, 46].

In addition, small nanoparticles incur manufacturability limitations in terms of drug load since the efficiency of encapsulating free drugs depends on the nanoparticle size [47, 48, 49, 50, 51, 52, 53, 54, 9]. For instance, we refer to the preparation of doxorubicin-loaded albumin nanoparticles in [47], as doxorubicin is one of the most widely used antineoplastic agents [55]. The minimum nanoparticle size produced in [47] is 128 nm and was associated with 58% entrapment efficiency. However, based on our recommendation of using lower ligand density and moderate diameter of 334 nm, the entrapment efficiency could reach up to 78%. Hence, avoiding the unnecessary decrease in nanoparticle size potentially removes a fundamental constraint that hinders the development of efficiently drug-loaded nanocarriers.

The robustness of the optimal design with respect to key tumor properties was then examined by studying the interaction among different parameters (Figure 4). The results show that nanoparticle accumulation predominantly depends on the nanoparticle design rather than on tumor vessels properties such as receptor density, blood viscosity, and temperature.

The results indicate that maximizing nanoparticle accumulation is not optimal with respect to the tumor diameter reduction. Larger nanoparticles are needed to yield better tumor regression due to the associated high drug load. This was confirmed by running a study that uses a drug of lower efficacy. Results showed that the minimizer of tumor diameter is larger. Therefore, the optimal design is not unique; however, a range of optimal values can be recommended. This range is bounded by the maximizer of nanoparticle accumulation and minimizers of tumor diameter, where a tradeoff between the two objective functions exist. Depending on the patient status and clinical evaluation, an optimal solution can be selected to satisfy the weight given for each treatment attribution (fast tumor size reduction versus low systemic toxicity). In contrast, when the drug efficacy is high, less drug load per nanoparticle is required, and the width of the tradeoff range decreases. We increased the drug efficacy until the minimizer of tumor diameter is smaller than the maximizer of tumor accumulation. If the drug efficacy is high, smaller nanoparticles are expected to yield better tumor shrinkage because they distribute more evenly. These results are consistent with [17, 1].

The results motivated another study to find the drug efficacy at which minimizing tumor diameter is tied to maximizing nanoparticle accumulation. If this drug efficacy exists, nanoparticles can be designed to eliminate anticipated tradeoffs between the desired treatment attributes. Therefore, we formulated an optimization

problem to find the drug efficacy that minimizes the difference between the two optimal designs. The complexity of the optimization problem leads us to synthesize a surrogate model using kriging metamodeling. The solution of the optimization problem indicates that a drug efficacy that is 4.6 times higher than the original value yields a minimal difference between the two optimal diameter values.

The analyses presented here are based on several assumptions. First, some biological parameters, such as hematocrit and drug diffusivity, were held constant. In reality, these parameters may vary by cancer type and tissue morphology and have an impact on the nanoparticle pharmacokinetics [36, 56]. Future studies will use probability density functions to capture these variations and produce more robust designs that could be used for a wider range of tumors. In addition, tumor size at the beginning of the treatment may affect the optimal solution. Therefore, future work will study the impact of tumor size on the response. Finally, shape has an effect on nanoparticle distribution and therapeutic potential [22, 29]. This study shows that the integration of optimization in the design process makes it possible to investigate the efficiency of different nanoparticle shapes, exploring new design trends that may lower the treatment toxicity while eradicating the tumor at a faster rate.

## 5 Conclusion

In this study, the design of drug-carrying nanoparticles is optimized to maximize tumor regression and minimize the treatment toxicity. Tumor regression is quantified as the percentage change of tumor diameter to that at the beginning of the treatment. The treatment toxicity is measured as the fraction of the injected nanoparticles that accumulate in the tumor. The optimal nanoparticle designs obtained provide a basis for further experimental and computational investigations. The study sheds light on design practices that increase nanoparticle circulation time while maintaining large drug encapsulation efficiency. This work lays a foundation to quantitatively evaluate preclinical nanoparticle-based drug delivery trials and support decisions in precision medicine where optimal solutions are required on a patient-specific basis.

## Author contributions statement

IC developed the optimization model and obtained the results. HBF and MK jointly developed the strategy for the project. IC wrote the manuscript, with input from HBF and MK. All authors approved the final manuscript.

## References

- [1] L. T. Curtis, M. Wu, J. Lowengrub, P. Decuzzi, and H. B. Frieboes, "Computational modeling of tumor response to drug release from vasculature-bound nanoparticles," *PLoS One*, 10(12), 1–17, 2015.
- [2] M. Martinez-Carmona, D. Lozano, M. Colilla, and M. Vallet-Regi, "Lectin-conjugated ph-responsive mesoporous silica nanoparticles for targeted bone cancer treatment," *Acta Biomater*, 65, 393–404, 2018.
- [3] R. Toy, E. Hayden, C. Shoup, H. Baskaran, and E. Karathanasis, "The effects of particle size, density and shape on margination of nanoparticles in microcirculation," *Nanotechnology*, 22(11), p. 115101, 2011.
- [4] P. Charoenphol, S. Mocherla, D. Bouis, K. Namdee, D. J. Pinsky, and O. Eniola-Adefeso, "Targeting therapeutics to the vascular wall in atherosclerosis-carrier size matters," *Atherosclerosis*, 217(2), 364–370, 2011.
- [5] V. R. S. Patil, C. J. Campbell, Y. H. Yun, S. M. Slack, and D. J. Goetz, "Particle diameter influences adhesion under flow," *Biophysical Journal*, 80, 1733–1743, 2001.
- [6] P. Decuzzi and M. Ferrari, "The adhesive strength of non-spherical particles mediated by specific interactions," *Biomaterials*, 27(30), 5307–14, 2006.
- [7] D. P. Boso, S. Y. Lee, M. Ferrari, B. A. Schrefler, and P. Decuzzi, "Optimizing particle size for targeting diseased microvasculature: from experiments to artificial neural networks," *Int J Nanomedicine*, 6, 1517–26, 2011.
- [8] I. Rostami, Z. Zhao, Z. Wang, W. Zhang, Y. Zhong, Q. Zeng, X. Jia, and Z. Hu, "Peptide-conjugated pegylated pamam as a highly affinitive nanocarrier towards her2-overexpressing cancer cells," *RSC Advances*, 6(109), 107337–107343, 2016.

- [9] H. Vardhan, P. Mittal, S. K. Adena, and B. Mishra, “Long-circulating polyhydroxybutyrate-co-hydroxyvalerate nanoparticles for tumor targeted docetaxel delivery: Formulation, optimization and in vitro characterization,” *Eur J Pharm Sci*, 99, 85–94, 2017.
- [10] S. Joshi, J. R. Cooke, D. K. Chan, J. A. Ellis, S. S. Hossain, R. P. Singh-Moon, M. Wang, I. J. Bigio, J. N. Bruce, and R. M. Straubinger, “Liposome size and charge optimization for intraarterial delivery to gliomas,” *Drug Deliv Transl Res*, 6(3), 225–33, 2016.
- [11] R. X. Zhang, T. Ahmed, L. Y. Li, J. Li, A. Z. Abbasi, and X. Y. Wu, “Design of nanocarriers for nanoscale drug delivery to enhance cancer treatment using hybrid polymer and lipid building blocks,” *Nanoscale*, 9, 1334–1355, 2017.
- [12] P. Decuzzi, S. Lee, B. Bhushan, and M. Ferrari, “A theoretical model for the margination of particles within blood vessels,” *Annals of Biomedical Engineering*, 33(2), 179–190, 2005.
- [13] V. Cristini, J. Lowengrub, and Q. Nie, “Nonlinear simulation of tumor growth,” *J Math Biol*, 46(3), 191–224, 2003.
- [14] S. R. McDougall, A. R. A. Anderson, and M. A. J. Chaplain, “Mathematical modelling of dynamic adaptive tumour-induced angiogenesis: Clinical implications and therapeutic targeting strategies,” *Journal of Theoretical Biology*, 241(3), 564–589, 2006.
- [15] P. Macklin, S. McDougall, A. R. Anderson, M. A. Chaplain, V. Cristini, and J. Lowengrub, “Multiscale modelling and nonlinear simulation of vascular tumour growth,” *J Math Biol*, 58(4–5), 765–98, 2009.
- [16] M. Wu, H. B. Frieboes, S. R. McDougall, M. A. Chaplain, V. Cristini, and J. Lowengrub, “The effect of interstitial pressure on tumor growth: coupling with the blood and lymphatic vascular systems,” *J Theor Biol*, 320, 131–51, 2013.
- [17] H. B. Frieboes, M. Wu, J. Lowengrub, P. Decuzzi, and V. Cristini, “A computational model for predicting nanoparticle accumulation in tumor vasculature,” *PLoS ONE*, 8(2), p. e56876, 2013.
- [18] A. L. van de Ven, M. Wu, J. Lowengrub, S. R. McDougall, M. A. Chaplain, V. Cristini, M. Ferrari, and H. B. Frieboes, “Integrated intravital microscopy and mathematical modeling to optimize nanotherapeutics delivery to tumors,” *AIP Adv*, 2(1), p. 11208, 2012.
- [19] M. Wu, H. B. Frieboes, M. A. Chaplain, S. R. McDougall, V. Cristini, and J. S. Lowengrub, “The effect of interstitial pressure on therapeutic agent transport: coupling with the tumor blood and lymphatic vascular systems,” *J Theor Biol*, 355, 194–207, 2014.
- [20] C. G. England, C. F. Ng, V. van Berkel, and H. B. Frieboes, “A review of pharmacological treatment options for lung cancer: Emphasis on novel nanotherapeutics and associated toxicity,” *Current Drug Targets*, 15, 1057–1087, 2015.
- [21] L. T. Curtis and H. B. Frieboes, *The Tumor Microenvironment as a Barrier to Cancer Nanotherapy*, pp. 165–190. Cham: Springer International Publishing, 2016.
- [22] I. M. Chamseddine and M. Kokkolaras, “Nanoparticle optimization for enhanced targeted anticancer drug delivery,” *J Biomech Eng*, 140(4), 2018.
- [23] P. Decuzzi, R. Pasqualini, W. Arap, and M. Ferrari, “Intravascular delivery of particulate systems: does geometry really matter?,” *Pharm Res*, 26(1), 235–43, 2009.
- [24] N. P. Truong, M. R. Whittaker, C. W. Mak, and T. P. Davis, “The importance of nanoparticle shape in cancer drug delivery,” *Expert Opin Drug Deliv*, 12(1), 129–42, 2015.
- [25] M. Sikkandhar, A. Nedumaran, R. Ravichandar, S. Singh, I. Santhakumar, Z. Goh, S. Mishra, G. Archunan, B. Gulyas, and P. Padmanabhan, “Theranostic probes for targeting tumor microenvironment: An overview,” *International Journal of Molecular Sciences*, 18(1036), 2017.
- [26] S. Le Digabel, “Algorithm 909: Nomad: Nonlinear optimization with the mads algorithm,” *ACM Transactions on Mathematical Software*, 37(4), 1–15, 2011.
- [27] C. Audet and J. Dennis, Jr., “Mesh adaptive direct search algorithms for constrained optimization,” *SIAM Journal on Optimization*, 17(1), 188–217, 2006.
- [28] C. Audet, M. Kokkolaras, S. Le Digabel, and B. Talgorn, “Order-based error for managing ensembles of surrogates in mesh adaptive direct search,” *Journal of Global Optimization*, 70, 645–675, 2018.
- [29] A. Sen Gupta, “Role of particle size, shape, and stiffness in design of intravascular drug delivery systems: insights from computations, experiments, and nature,” *Wiley Interdiscip Rev Nanomed Nanobiotechnol*, 8(2), 255–70, 2016.
- [30] P. Hermann, M. Armant, E. Brown, M. Rubio, H. Ishihara, D. Ulrich, R. Caspary, F. Lindberg, R. Armitage, C. Maliszewski, G. Delespesse, and M. Sarfati, “The vitronectin receptor and its associated cd47 molecule mediates proinflammatory cytokine synthesis in human monocytes by interaction with soluble cd23,” *The Journal of Cell Biology*, 144(4), 767–775, 1999.

- [31] L. Wang, D. Pan, Q. Yan, and Y. Song, "Activation mechanisms of  $\alpha_v\beta_3$  integrin by binding to fibronectin: A computational study," *Protein Science*, 26(6), 1124–1137, 2017.
- [32] K. Yokoyama, X.-P. Zhang, L. Medved, and Y. Takada, "Specific binding of integrin  $\alpha_v\beta_3$  to the fibrinogen  $\gamma$  and  $\alpha_e$  chain c-terminal domains," *Biochemistry*, 38(18), 5872–5877, 1999.
- [33] Y.-J. Kang, K. Forbes, J. Carver, and J. D. Aplin, "The role of the osteopontin-integrin  $\alpha_v\beta_3$  interaction at implantation: functional analysis using three different in vitro models," *Human Reproduction*, 29(4), 739–749, 2014.
- [34] D. Bertsimas, D. B. Brown, and C. Caramanis, "Theory and applications of robust optimization," *SIAM Review*, 53(3), 464–501, 2011.
- [35] S. Lophaven, H. B. Nielsen, and J. Sondergaard, "Dace – a matlab kriging toolbox," 2002.
- [36] L. B. Sims, M. K. Huss, H. B. Frieboes, and J. M. Steinbach-Rankins, "Distribution of PLGA-modified nanoparticles in 3D cell culture models of hypo-vascularized tumor tissue," *J Nanobiotechnology*, 15(1), p. 67, 2017.
- [37] L. T. Curtis, P. Rychahou, Y. Bae, and H. B. Frieboes, "A computational/experimental assessment of antitumor activity of polymer nanoassemblies for ph-controlled drug delivery to primary and metastatic tumors," *Pharm Res*, 33(10), 2552–64, 2016.
- [38] J. W. Hickey, J. L. Santos, J. M. Williford, and H. Q. Mao, "Control of polymeric nanoparticle size to improve therapeutic delivery," *J Control Release*, 219, 536–547, 2015.
- [39] R. Kadian, "Nanoparticles: A promising drug delivery approach," *Asian Journal of Pharmaceutical and Clinical Research*, 11(1), p. 30, 2018.
- [40] S. Cao, Y. Jiang, C. N. Levy, S. M. Hughes, H. Zhang, F. Hladik, and K. A. Woodrow, "Optimization and comparison of cd4-targeting lipid-polymer hybrid nanoparticles using different binding ligands," *J Biomed Mater Res A*, 2017.
- [41] A. C. Lima, C. Alvarez-Lorenzo, and J. F. Mano, "Design advances in particulate systems for biomedical applications," *Adv Healthc Mater*, 5(14), 1687–723, 2016.
- [42] D. Guo, C. Shi, X. Wang, L. Wang, S. Zhang, and J. Luo, "Riboflavin-containing telodendrimer nanocarriers for efficient doxorubicin delivery: High loading capacity, increased stability, and improved anticancer efficacy," *Biomaterials*, 141, 161–175, 2017.
- [43] G. Schmid, W. G. Kreyling, and U. Simon, "Toxic effects and biodistribution of ultrasmall gold nanoparticles," *Arch Toxicol*, 91(9), 3011–3037, 2017.
- [44] C. Foged, B. Brodin, S. Frokjaer, and A. Sundblad, "Particle size and surface charge affect particle uptake by human dendritic cells in an in vitro model," *International Journal of Pharmaceutics*, 298(2), 315–322, 2005.
- [45] S. E. A. Gratton, P. A. Ropp, P. D. Pohlhaus, J. C. Luft, V. J. Madden, M. E. Napier, and J. M. DeSimone, "The effect of particle design on cellular internalization pathways," *Proceedings of the National Academy of Sciences*, 105(33), 11613–11618, 2008.
- [46] S. Muro, C. Garnacho, J. A. Champion, J. Leferovich, C. Gajewski, E. H. Schuchman, S. Mitragotri, and V. R. Muzykantov, "Control of endothelial targeting and intracellular delivery of therapeutic enzymes by modulating the size and shape of icam-1-targeted carriers," *Molecular Therapy*, 16(8), 1450–1458, 2008.
- [47] L. Li, X. Zhao, C. Yang, H. Hu, M. Qiao, and D. Chen, "Preparation and optimization of doxorubicin-loaded albumin nanoparticles using response surface methodology," *Drug Dev Ind Pharm*, 37(10), 1170–80, 2011.
- [48] A. A. Elsaid Ali, M. Taher, and F. Mohamed, "Microencapsulation of alpha-mangostin into PLGA microspheres and optimization using response surface methodology intended for pulmonary delivery," *Journal of Microencapsulation*, 30(8), 728–740, 2013.
- [49] S. Asghar, J. M. M. Salmani, W. Hassan, Y. Xie, F. Meng, Z. Su, M. Sun, Y. Xiao, and Q. Ping, "A facile approach for crosslinker free nano self assembly of protein for anti-tumor drug delivery: Factors' optimization, characterization and in vitro evaluation," *European Journal of Pharmaceutical Sciences*, 63, 53–62, 2014.
- [50] P. Chaubey, R. R. Patel, and B. Mishra, "Development and optimization of curcumin-loaded mannosylated chitosan nanoparticles using response surface methodology in the treatment of visceral leishmaniasis," *Expert Opin Drug Deliv*, 11(8), 1163–81, 2014.
- [51] P. Boonyasirisri, U. Nimmannit, P. Rojsitthisak, S. Bhunchu, and P. Rojsitthisak, "Optimization of curcuminoid-loaded PLGA nanoparticles using box-behnken statistical design," *Journal of Nano Research*, 33, 60–71, 2015.
- [52] M. A. Akl, A. Kartal-Hodzic, T. Oksanen, H. R. Ismael, M. M. Afouna, M. Yliperttula, A. M. Samy, and T. Viitala, "Factorial design formulation optimization and in vitro characterization of curcumin-loaded PLGA nanoparticles for colon delivery," *Journal of Drug Delivery Science and Technology*, 32, 10–20, 2016.
- [53] R. de Oliveira Pedro, F. M. Goycoolea, S. Pereira, C. C. Schmitt, and M. G. Neumann, "Synergistic effect of quercetin and ph-responsive deae-chitosan carriers as drug delivery system for breast cancer treatment," *Int J Biol Macromol*, 106, 579–586, 2018.

- 
- [54] K. Rajpoot and S. K. Jain, "Colorectal cancer-targeted delivery of oxaliplatin via folic acid-grafted solid lipid nanoparticles: preparation, optimization, and in vitro evaluation," *Artif Cells Nanomed Biotechnol*, pp. 1–12, 2017.
- [55] L. Brannon-Peppas and J. O. Blanchette, "Nanoparticle and targeted systems for cancer therapy," *Adv Drug Deliv Rev*, 56(11), pp. 1649–59, 2004.
- [56] L. B. Sims, K. C. Curry, S. Parupalli, G. Horner, H. B. Frieboes, and J. M. Steinbach-Rankins, "Efficacy of surface-modified PLGA nanoparticles to treat cervical cancer." (in press), 2018.